

Map Reconstruction in UAV Networks via Fusion of Radio and Depth Measurements

Omid Esrafilian, Rajeev Gangula, and David Gesbert

Communication Systems Department, EURECOM, Sophia Antipolis, France

Email:{esrafilian, gangula, gesbert}@eurecom.fr

Abstract—In this work, we develop an algorithm to construct radio maps that can predict the received signal strength between a UAV-mounted base station and arbitrary ground users. The novelty of the work lies in the fact that these maps are constructed by fusing UAV-user radio signal strength measurements, and depth information of the surrounding environment which is obtained by an on-board laser range finder sensor. The proposed approach exploits both line-of-sight (LoS) and non-line-of-sight (NLoS) nature of UAV-user channels and depth information to first obtain the 3D map of the city and then later use it to estimate the radio map. Numerical results demonstrate the significant gain brought by the fusion of radio and depth measurements as opposed to a system which only relies on radio measurements.

Index Terms—UAV, drone, 3D map, learning, radio map

I. INTRODUCTION

Recently there has been an increased interest in the design of flying radio access networks (FRANs), where wireless connectivity to ground users is provided by aerial base stations (BSs) or access points (APs) that can be mounted on low altitude unmanned aerial vehicles (UAVs) [1], [2]. FRANs can compliment the existing terrestrial radio access networks with the added advantage that the UAV BS locations can be changed dynamically to maximize the network performance [3], [4].

In UAV BS placement or trajectory optimization problems, UAV-user channels play a crucial role, and often these are unknown before deployment. While simple pathloss models can be used in rural and suburban areas where UAV-user links predominantly have line-of-sight (LoS) conditions, in urban environments with number of buildings it is known that UAV-user links often switch between LoS and non-line-of-sight (NLoS) conditions due to the building blockages depending on the UAV and user locations [5], [6]. In such scenarios, radio maps which describe the average channel gains for all combinations of UAV and user locations are needed.

The work in [7] considers the problem of radio map estimation from the received signal strength (RSS) measurements collected from the ground users who are served by the UAV. A segmented pathloss model that differentiates between LoS and NLoS conditions is used. The authors formulate the problem as a joint classification and regression problem and an expectation-maximization (EM) like algorithm is proposed to estimate the radio map. However, the radio map for each user

has to be re-estimated every time the user location is changed. This drawback can be alleviated by exploiting the fact that the radio map ultimately depends on the fine-grained building topology which contains the information about LoS/NLoS classification of UAV-user channels as shown in [8].

However, in situations where 3D map of the environment is not readily available, different sensors on the UAV can be used for the map reconstruction, examples include camera, Lidar etc. An interesting idea is proposed in [9], where UAV BS can use the signal strength measurements from the users to reconstruct the 3D map. The authors first classify the data into LoS/NLoS segments based on statistical techniques and then use this information to construct the map. However, UAV needs to collect measurements at various locations from a large number of ground users to construct the 3D map.

In this work, we aim to estimate the radio map with a UAV BS via constructing the 3D map of the environment and learning the channel parameters in LoS and NLoS segments. We assume that the UAV BS has an extra on-board laser range finder sensor which allows it to obtain depth information in the surrounding environment. Depth information consists of distances from the surrounding objects in the sensor's range. This information is then fused with radio measurements collected from the users to construct the 3D map. The extra sensor alleviates the drawbacks of needing: a) re-estimation of the radio map once the user location or UAV altitude changes [7], b) radio measurement collection from large number of users to construct the 3D map as in [9]. To the best of our knowledge, the problem of radio map estimation with a UAV BS by fusing depth and RSS measurements has not been addressed before. Specifically, our contributions are as follows:

- In a limited UAV mission time, by exploiting both depth information and RSS measurements from a limited number of ground users, we estimate the 3D city map and the channel parameters.
- The 3D map along with the learned channel parameters are then used to estimate a high-quality radio map.

II. SYSTEM MODEL

We consider a scenario where a UAV-mounted BS is serving K outdoor ground level users in an urban environment comprising a number of city buildings. The environment is denoted by a cuboid $\mathcal{M} = [0, a] \times [0, a] \times [0, h] \in \mathbb{R}^3$, where h represents the UAV flying altitude and it is larger than the

maximum height of the buildings in the considered area. The users are scattered all over the city and $\mathbf{u}_k = [x_k, y_k, 0]^T \in \mathcal{M}$, $k \in \{1, \dots, K\}$ denotes the k -th user's location. The users are static and their locations are known. We intend to build the radio map of any given user i.e., the signal strength from the user to the UAV which can be at various points in \mathcal{M} . To construct such maps, the UAV BS not only uses radio measurements from ground users but it is also aided with an on-board 3D laser range finder sensor (i.e. Lidar) which will be useful in the environment mapping.

A. UAV model

The UAV mission lasts for a duration of T during which the UAV follows a trajectory of length L meters with a constant velocity. We assume that the time period $[0, T]$ is discretized into N equal length intervals, each of duration $\delta = T/N$, indexed by $n = 1, \dots, N$. In the n -th interval, the UAV/drone position is denoted by $\mathbf{v}_n = [x_n, y_n, h]^T \in \mathcal{M}_h$, where $\mathcal{M}_h = [0, a] \times [0, a] \times h$. We assume that the drone is equipped with a GPS receiver, hence $\mathbf{v}_n, \forall n$ is known. While following this trajectory, the UAV collects received signal strength (RSS) measurements from the users and depth measurements from the laser scanner to map the environment.

B. Measurement collection

Let us denote the arbitrary trajectory followed by the UAV during the mission by a sequence $\mathbf{v}_{1:N} = \{\mathbf{v}_n, n \in [1, N]\}$. We assume that the UAV collects RSS measurements from all ground users in each time slot and depth measurements are obtained by the laser scanner on slots where $(n \bmod \kappa) = 0$, $\kappa > 1, \kappa \in \mathbb{Z}^+$. This assumption is used to model the fact that in general radio measurements can be obtained at a rate much faster than the laser scanner measurements as the laser needs some time to map the environment.

Let $g_{n,k}$ represent the channel gain or RSS measurement (in dB scale) obtained from the k -th user by the UAV in the n -th interval. Using the segmented pathloss model that is suitable for air-to-ground channels in urban environments with buildings [6], [7], we have

$$g_{n,k} = \begin{cases} \lambda(\boldsymbol{\theta}_{\text{LoS}}, \mathbf{v}_n, \mathbf{u}_k) + \eta_{n,k,\text{LoS}} & \text{if LoS} \\ \lambda(\boldsymbol{\theta}_{\text{NLoS}}, \mathbf{v}_n, \mathbf{u}_k) + \eta_{n,k,\text{NLoS}} & \text{if NLoS} \end{cases}, \quad (1)$$

where

$$\lambda(\boldsymbol{\theta}_s, \mathbf{v}_n, \mathbf{u}_k) = \beta_s - \alpha_s 10 \log_{10}(\|\mathbf{u}_k - \mathbf{v}_n\|), \quad (2)$$

$\boldsymbol{\theta}_s = [\alpha_s, \beta_s]^T$, $s \in \{\text{LoS}, \text{NLoS}\}$, α_s is the pathloss exponent, β_s is the channel gain offset, and $\eta_{n,k,s}$ represents shadowing effect with zero-mean Gaussian distribution with variance σ_s^2 .

Moreover, the UAV collects depth measurements by scanning the environment using its laser range finder. Each scan of the laser range finder in a time slot contains J depth information measurements of the observed objects in the environment. The set of depth measurements at time interval n , such that $(n \bmod \kappa) = 0$, is denoted as $\chi_n^d = \{\gamma_{n,1}, \dots, \gamma_{n,J}\}$. The j -th depth measurement is denoted by a tuple $\gamma_{n,j} =$

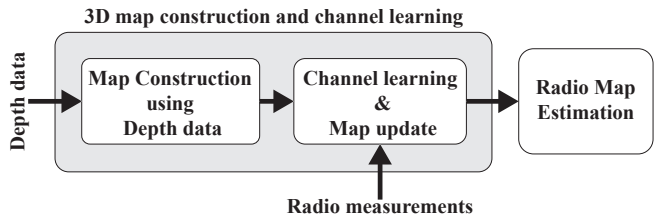


Fig. 1: Different steps in the radio map construction algorithm.

$(r_{n,j}, \phi_{n,j}, \psi_{n,j})$, where $0 \leq r_{n,j} \leq r_{\max}$, $0 \leq \phi_{n,j} \leq 2\pi$, $0 \leq \psi_{n,j} \leq \psi_{\max}$ are, respectively, the distance, the azimuthal, and the polar angle of the observed object with respect to the UAV. The maximum range of the sensor is represented by r_{\max} , and ψ_{\max} is the field of view of the sensor. Note that, we assume the sensor is faced downwards to scan the buildings on the ground. In this paper, we neglect the noise of the depth measurements since most of the laser range finders can provide highly accurate measurements.

C. Problem formulation

The aim of the UAV mission is to construct the radio map of any given users i.e., the RSS estimate of UAV-user channels at any arbitrary UAV location in \mathcal{M} using the above mentioned measurement collection process. To construct the radio map for a user, we first need to determine the status of the UAV-user link as LoS/NLoS and then using (1), the channel gain in that segment can be estimated. The classification task can be done by exploiting the 3D map of the environment, since if we know the location of the blocking objects we can determine the status of any UAV-user link. However, the 3D map of the environment is not available and needs to be constructed as well. The radio channel parameters also need to be learned from the collected radio measurements. The steps in the proposed radio map reconstruction algorithmic process is illustrated in Fig. 1.

III. 3D MAP RECONSTRUCTION

To construct the 3D map, we follow occupancy grid representation approach. The map of the environment, \mathcal{M} is partitioned into M individual grids of equal volume. The center of the i -th grid is denoted by $\mathbf{c}_i \in \mathcal{M}$, $i \in [1, M]$. The i -th grid is associated with a binary random variable m_i representing whether the grid is occupied or empty. Occupancy grid algorithms compute approximate posterior estimates for these random variables. More specifically, our goal is to calculate the posterior distribution

$$p(\mathcal{M} | \chi_{1:N}, \mathbf{v}_{1:N}), \quad (3)$$

where $\chi_{1:N}$ contains all the collected measurements in the mission duration (i.e. radio and depth), $\mathbf{v}_{1:N}$ denotes the corresponding UAV locations for taking these measurements. We assume that the map does not change with time (static environment) and the grids are independent. Therefore,

$$p(\mathcal{M} | \chi_{1:N}, \mathbf{v}_{1:N}) = \prod_i p(m_i | \chi_{1:N}, \mathbf{v}_{1:N}). \quad (4)$$

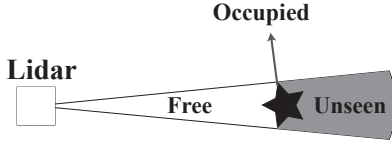


Fig. 2: An example of the sensor model.

To compute this, we follow the steps as shown in Fig. 1.

A. Map construction using depth measurements

We first use the depth measurements to construct a 3D model of the city which to be updated later by the radio measurements. Based on the laser range finder measurements, the grid probabilities are updated by [10]

$$\frac{p(m_i|\chi_{1:N}^d, \mathbf{v}_{1:N})}{1 - p(m_i|\chi_{1:N}^d, \mathbf{v}_{1:N})} = \prod_{n=1}^N \prod_{j=1}^J \frac{p(m_i|\gamma_{n,j}, \mathbf{v}_n)}{1 - p(m_i|\gamma_{n,j}, \mathbf{v}_n)} \times \frac{p(m_i)}{1 - p(m_i)}, \quad (5)$$

where we assume that the measurements are independent, $p(m_i)$ represents the prior information, and the probability density function (PDF) $p(m_i|\gamma_{n,j}, \mathbf{v}_n)$ is the sensor model which provides information about the map given a sensor reading caused by an object in the environment. Note that on time slots where the depth measurement is not available i.e., $(n \bmod \kappa \neq 0)$, we have $p(m_i|\gamma_{n,j}, \mathbf{v}_n) = 0.5$. For a given depth measurement $\gamma_{n,j} = (r_{n,j}, \phi_{n,j}, \psi_{n,j})$, let us denote \mathcal{G} as a set of all grid cells indices which lie on the straight line between the sensor (UAV) and the detected object. The sensor model for this measurement is given by [10]

$$\forall i \in \mathcal{G}, p(m_i|\gamma_{n,j}, \mathbf{v}_n) = \begin{cases} p_{free} & \text{if } \|\mathbf{c}_i - \mathbf{v}_n\| < r_{n,j} \\ p_{occ} & \text{if } \|\mathbf{c}_i - \mathbf{v}_n\| = r_{n,j} \\ 0.5 & \text{if } \|\mathbf{c}_i - \mathbf{v}_n\| > r_{n,j}, \end{cases} \quad (6)$$

which says that, for all the grids between the sensor and the detected object, there is a high probability that there is no obstacle, then we assign a low probability of occupancy $p_{free} < 0.5$ to all of these grids. Very close to the object it is high likely that there is an obstacle. So, the grids around the object are considered occupied with the probability of $p_{occ} > 0.5$. Since the sensor cannot see behind the object, then we have no certain information about the grids behind the object. Fig. 2 shows an example of the sensor model assigned to each measurements obtained by the laser scanner.

This map will be fused with radio measurements in the next step of the algorithm to learn the channel parameters and then will be enhanced by the radio measurements.

B. Radio measurement classification and channel learning

In order to use the collected RSS measurements for the purpose of 3D map enhancement, we first need to classify them into LoS and NLoS categories. The problem of joint classification and channel parameters learning has been studied in [7]. However, the work in [7] depends only on channel

measurement statistics and does not have any prior information regarding the 3D map. Since we have already an updated map information which is obtained by the depth measurements, we feed this information to our algorithm to jointly learn the channel parameters and classify the radio measurements. The proposed EM-based algorithm accepts the map information (coming from previous section) and RSS measurements as inputs and returns the labels of the RSS measurements as LoS/NLoS and the learned channel parameters as outputs.

Let $w_{n,k} \in \{\text{LoS}, \text{NLoS}\}$ be a latent binary random variable which determines the LoS/NLoS label of the RSS measurement $g_{n,k}$ as defined in (1). We similarly define another binary random variable $\rho_{n,k} \in \{\text{LoS}, \text{NLoS}\}$ which determines the label of each measurement from the constructed occupancy grid map using the depth information. The joint PDF of $g_{n,k}$ can then be written as

$$p(g_{n,k}, w_{n,k}, \rho_{n,k}) = p(g_{n,k}|w_{n,k}, \rho_{n,k}) p(w_{n,k}|\rho_{n,k}) p(\rho_{n,k}). \quad (7)$$

Given two variables s and \hat{s} , where each one takes on the values in the set $\{\text{LoS}, \text{NLoS}\}$, we can write

$$p(g_{n,k}, w_{n,k} = s, \rho_{n,k} = \hat{s}) = p(g_{n,k}, s, \hat{s}) \tau_{s,\hat{s}} \pi_{n,k,\hat{s}}, \quad (8)$$

where $p(g_{n,k}, s, \hat{s}) \triangleq p(g_{n,k}|w_{n,k} = s, \rho_{n,k} = \hat{s})$, $\tau_{s,\hat{s}} \triangleq p(w_{n,k} = s|\rho_{n,k} = \hat{s})$, and $\pi_{n,k,\hat{s}} \triangleq p_{n,k}(\rho_{n,k} = \hat{s})$. According to (1), $p(g_{n,k}, s, \hat{s})$ has the following distribution

$$p(g_{n,k}, s, \hat{s}) \sim \mathcal{N}(\lambda(\boldsymbol{\theta}_s, \mathbf{v}_n, \mathbf{u}_k), \sigma_s^2), s \in \{\text{LoS}, \text{NLoS}\}, \quad (9)$$

which only depends on the latent variable $w_{n,k}$ and doesn't depend on \hat{s} . The marginal probability $\tau_{s,\hat{s}}$, has the following property

$$\sum_s \tau_{s,\hat{s}} = 1, \forall \hat{s} \in \{\text{LoS}, \text{NLoS}\}. \quad (10)$$

The probability that the measurement $g_{n,k}$ belongs to segment \hat{s} , denoted by $\pi_{n,k,\hat{s}}$, is obtained by leveraging the occupancy grid map as follows

$$\pi_{n,k,\hat{s}} = \begin{cases} 1 - \max_{i \in \mathcal{G}(\mathbf{v}_n, \mathbf{u}_k)} p(m_i|\chi_{1:N}^d, \mathbf{v}_{1:N}) & \text{if } \hat{s} = \text{LoS} \\ \max_{i \in \mathcal{G}(\mathbf{v}_n, \mathbf{u}_k)} p(m_i|\chi_{1:N}^d, \mathbf{v}_{1:N}) & \text{if } \hat{s} = \text{NLoS} \end{cases}, \quad (11)$$

where $\mathcal{G}(\mathbf{v}_n, \mathbf{u}_k)$ is a set of grids which lie on the straight line between the UAV at location \mathbf{v}_n and the k -th user. The occupancy probability of grid m_i based on the depth measurements, $p(m_i|\chi_{1:N}^d, \mathbf{v}_{1:N})$, is obtained from (5). Equation (11) stems from the definition of the NLoS link, i.e, a link between UAV and user is considered as NLoS if it is obstructed by at least one blocking object. So, even if one grid is occupied along the link, we consider it as a NLoS link.

Assuming that RSS measurements conditioned on channel parameters and user positions are independent and identically distributed¹, the log-likelihood of the unknown parameters

¹This amounts to assuming the shadowing coefficients are independent over successive UAV locations, which is a classical assumption, see for e.g. [7].

$\xi = \{\theta_s, \sigma_s, \tau_{s,\hat{s}}; \forall s, \hat{s}\}$ is given by

$$\begin{aligned} \mathcal{L}(\xi) &= \sum_{n,k} \log p(g_{n,k}; \xi) \\ &= \sum_{n,k} \log \sum_{w_{n,k}, \rho_{n,k}} p(g_{n,k}, w_{n,k}, \rho_{n,k}; \xi) \end{aligned} \quad (12)$$

For each measurement, let $Q(w_{n,k}, \rho_{n,k})$ be a joint distribution over $w_{n,k}$ and $\rho_{n,k}$. We can then reformulate (12) as

$$\begin{aligned} \mathcal{L}(\xi) &= \sum_{n,k} \log \sum_{w_{n,k}, \rho_{n,k}} Q(w_{n,k}, \rho_{n,k}) \frac{p(g_{n,k}, w_{n,k}, \rho_{n,k}; \xi)}{Q(w_{n,k}, \rho_{n,k})} \\ &\geq \sum_{n,k} \sum_{w_{n,k}, \rho_{n,k}} Q(w_{n,k}, \rho_{n,k}) \log \frac{p(g_{n,k}, w_{n,k}, \rho_{n,k}; \xi)}{Q(w_{n,k}, \rho_{n,k})} \end{aligned} \quad (13)$$

The last step follows from Jensen's inequality. Now for any distributions Q , the formula (13) provides a lower bound on $\mathcal{L}(\xi)$. This bound can be tightened by choosing Q as follows

$$\begin{aligned} Q(w_{n,k}, \rho_{n,k}) &= \frac{p(g_{n,k}, w_{n,k}, \rho_{n,k}; \xi)}{\sum_{w_{n,k}, \rho_{n,k}} p(g_{n,k}, w_{n,k}, \rho_{n,k}; \xi)} \\ &= \frac{p(g_{n,k}, s, \hat{s}; \xi) \tau_{s,\hat{s}} \pi_{n,k,\hat{s}}}{\sum_{s,\hat{s}} p(g_{n,k}, s, \hat{s}; \xi) \tau_{s,\hat{s}} \pi_{n,k,\hat{s}}}. \end{aligned} \quad (14)$$

In this case, the step involving Jensen's inequality in (13) holds with equality and we have a tight lower bound on $L(\xi)$. Let $\Omega_{n,k,s,\hat{s}}$ denote the probability of $w_{n,k}, \rho_{n,k}$ taking the values s and \hat{s} , respectively, hence,

$$\Omega_{n,k,s,\hat{s}} \triangleq Q(w_{n,k} = s, \rho_{n,k} = \hat{s}).$$

Then the maximum log-likelihood estimation of ξ can be obtained by solving the following problem

$$\begin{aligned} \max_{\xi, \Omega_{n,k,s,\hat{s}}} & \sum_{n,k} \sum_{w_{n,k}, \rho_{n,k}} \Omega_{n,k,s,\hat{s}} \log \frac{p(g_{n,k}, s, \hat{s}; \xi) \tau_{s,\hat{s}} \pi_{n,k,\hat{s}}}{\Omega_{n,k,s,\hat{s}}} \\ \text{s.t.} & (10). \end{aligned} \quad (15)$$

Problem (15) is non-convex so challenging to solve. To deal with this difficulty, we instead find a sub-optimal solution by solving (15) iteratively. This algorithm iterates between two steps known as expectation and maximization, a.k.a. E-M steps. During the E-phase, the $\Omega_{n,k,s,\hat{s}}$ is computed by using (14) while fixing parameters ξ . In the M-step, problem (15) is solved only for parameters ξ by fixing $\Omega_{n,k,s,\hat{s}}$. We denote i as the iteration index of the algorithm and we assume that the process is repeated for I iterations.

Let $\xi^{(i)}$ be the parameters available from the i -th iteration, then during the E-step we have

$$\Omega_{n,k,s,\hat{s}}^{(i+1)} = \frac{p(g_{n,k}, s, \hat{s}; \xi^{(i)}) \tau_{s,\hat{s}}^{(i)} \pi_{n,k,\hat{s}}}{\sum_{s,\hat{s}} p(g_{n,k}, s, \hat{s}; \xi^{(i)}) \tau_{s,\hat{s}}^{(i)} \pi_{n,k,\hat{s}}}. \quad (16)$$

For the M-step, (15) can be reformulated as follows:

$$\begin{aligned} \max_{\xi^{(i)}} & \sum_{n,k} \sum_{s,\hat{s}} \Omega_{n,k,s,\hat{s}}^{(i+1)} \log \frac{p(g_{n,k}, s, \hat{s}; \xi^{(i)}) \tau_{s,\hat{s}} \pi_{n,k,\hat{s}}}{\Omega_{n,k,s,\hat{s}}^{(i+1)}} \\ \text{s.t.} & (10). \end{aligned} \quad (17)$$

where the objective function is concave. By setting the derivative of (17) with respect to $\xi^{(i)}$ to zero and solving, we find

$$\theta_s^{(i+1)} = \mathbf{A}_s^{-1} \mathbf{b}_s, \quad (18)$$

$$\sigma_s^{(i+1)} = \sqrt{\frac{\sum_{n,k} \sum_{s,\hat{s}} \Omega_{n,k,s,\hat{s}}^{(i+1)} \left(g_{n,k} - \lambda(\theta_s^{(i+1)}, \mathbf{v}_n, \mathbf{u}_k) \right)^2}{\sum_{n,k} \sum_{s,\hat{s}} \Omega_{n,k,s,\hat{s}}^{(i+1)}}}, \quad (19)$$

where

$$\begin{aligned} \mathbf{A}_s &= \begin{bmatrix} \sum_{n,k} \sum_{s,\hat{s}} \Omega_{n,k,s,\hat{s}}^{(i+1)} d_{n,k}^2 & \sum_{n,k} \sum_{s,\hat{s}} \Omega_{n,k,s,\hat{s}}^{(i+1)} d_{n,k} \\ \sum_{n,k} \sum_{s,\hat{s}} \Omega_{n,k,s,\hat{s}}^{(i+1)} d_{n,k} & \sum_{n,k} \sum_{s,\hat{s}} \Omega_{n,k,s,\hat{s}}^{(i+1)} \end{bmatrix}, \\ \mathbf{b}_s &= \begin{bmatrix} \sum_{n,k} \sum_{s,\hat{s}} \Omega_{n,k,s,\hat{s}}^{(i+1)} d_{n,k} g_{n,k} \\ \sum_{n,k} \sum_{s,\hat{s}} \Omega_{n,k,s,\hat{s}}^{(i+1)} g_{n,k} \end{bmatrix}, \end{aligned}$$

and $d_{n,k} = -10 \log_{10}(\|\mathbf{u}_k - \mathbf{v}_n\|)$. The value of $\tau_{s,\hat{s}}^{(i+1)}$ is computed as

$$\tau_{s,\hat{s}}^{(i+1)} = \frac{\sum_{n,k} \Omega_{n,k,s,\hat{s}}^{(i+1)}}{\sum_{n,k} \sum_{c \in \{\text{LoS}, \text{NLoS}\}} \Omega_{n,k,c,\hat{s}}^{(i+1)}}. \quad (20)$$

C. Map enhancement

In this step, we make use of the joint distribution of the labels $\Omega_{n,k,s,\hat{s}}$ to enhance the 3D map. The probability of a measurement $g_{n,k}$ belonging to LoS category is given by

$$\Omega_{n,k,\text{LoS}}^{(I)} = \sum_{\hat{s} \in \{\text{LoS}, \text{NLoS}\}} \Omega_{n,k,\text{LoS},\hat{s}}^{(I)}, \quad (21)$$

where $\Omega_{n,k,s,\hat{s}}^{(I)}$ is the marginal probability at the last iteration of the algorithm as described in Section III-B. Let $s_{n,k}$ be the label of the measurement $g_{n,k}$ that is obtained using hard classification as follows

$$s_{n,k} = \begin{cases} \text{LoS} & \text{if } \Omega_{n,k,\text{LoS}}^{(I)} > 0.5 \\ \text{NLoS} & \text{else} \end{cases}. \quad (22)$$

The LoS measurements will be used to improve the 3D map, as the LoS measurements indicate that there is no obstacle between the corresponding user and the UAV as illustrated in Fig. 3. Therefore, for a given UAV-user link which is LoS, grids that lie on the LoS line and also all the grids above the LoS line are high likely to be empty. We then assign the probability of occupancy $p_{free} < 0.5$ to these grids. Note that, since we assume that all the users are on the ground then there are no grids to be seen behind the users.

To update the 3D map with the radio measurements, we treat the map constructed using the depth information $p(\mathcal{M} | \chi_{1:N}^d, \mathbf{v}_{1:N})$ as a prior. Similar to (5), the updated map can be approximated as follows

$$\begin{aligned} \frac{p(m_i | \chi_{1:N}^d, \chi_{1:N}^r, \mathbf{v}_{1:N})}{1 - p(m_i | \chi_{1:N}^d, \chi_{1:N}^r, \mathbf{v}_{1:N})} &\approx \prod_{n=1}^N \prod_{k \in \mathcal{K}_n} \frac{p(m_i | g_{n,k}, \mathbf{v}_n)}{1 - p(m_i | g_{n,k}, \mathbf{v}_n)} \\ &\times \frac{p(m_i | \chi_{1:N}^d, \mathbf{v}_{1:N})}{1 - p(m_i | \chi_{1:N}^d, \mathbf{v}_{1:N})}, \end{aligned} \quad (23)$$

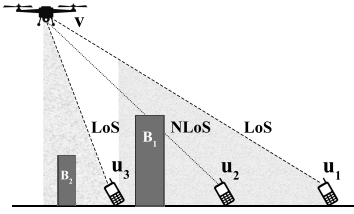


Fig. 3: LoS and NLoS radio measurements.

where \mathcal{K}_n is a set of user indices that are LoS to the UAV at the n -th time step, and $\chi_{1:N}^r$ is all of LoS radio measurements collected up to time step N . The probability $p(m_i|g_{n,k}, \mathbf{v}_n) = p_{free}$ for all the grids which are above or lie on the line between the UAV location \mathbf{v}_n and the k -th user, otherwise it is equal to 0.5.

IV. RADIO MAP ESTIMATION

Building on the estimated 3D map and the learned channel parameters, we now estimate the radio map for a given user and any UAV locations. To this end, we start by finding the LoS probability of the UAV-user link. To do this, the occupancy map, which was reconstructed in the previous section is used. Akin to section III-B, for any arbitrary UAV location $\mathbf{v} \in \mathcal{M}$, the LoS probability of the link between the UAV and the user located at $\mathbf{u} \in \mathbb{R}^2$ can be obtained as follows

$$p(\mathbf{v}, \mathbf{u}) = 1 - \max_{i \in \mathcal{G}(\mathbf{v}, \mathbf{u})} p(m_i | \chi_{1:N}^d, \chi_{1:N}^r, \mathbf{v}_{1:N}). \quad (24)$$

The estimated channel gain of the UAV-user link is given by

$$\hat{g}(\mathbf{v}, \mathbf{u}) = \begin{cases} \lambda(\theta_{\text{LoS}}^{(I)}, \mathbf{v}, \mathbf{u}) & \text{if } p(\mathbf{v}, \mathbf{u}) > 0.5 \\ \lambda(\theta_{\text{NLoS}}^{(I)}, \mathbf{v}, \mathbf{u}) & \text{else} \end{cases}. \quad (25)$$

V. NUMERICAL RESULTS

In this section, we provide numerical results to show the performance of the proposed algorithm. We consider a dense urban city neighborhood of size $600 \times 600 \text{ m}^2$, comprising buildings and regular streets as shown in Fig. 4. The height of the buildings is Rayleigh distributed in the range of 5 to 40 m [6]. The true propagation parameters are chosen as $\alpha_{\text{LoS}} = 2.5$, $\alpha_{\text{NLoS}} = 3.04$, $\beta_{\text{LoS}} = -30 \text{ dB}$, $\beta_{\text{NLoS}} = -35 \text{ dB}$ according to an urban micro scenario [11]. The variances of the shadowing components in LoS and NLoS scenarios are $\sigma_{\text{LoS}}^2 = 3 \text{ dB}$, and $\sigma_{\text{NLoS}}^2 = 5 \text{ dB}$, respectively. To construct the 3D map of the city and to learn the channel parameters, the UAV collects the radio measurements and the depth information while following a square trajectory of length 1600 m as shown in Fig. 4. The altitude of the UAV is fixed to 60 m during the course of its trajectory. The UAV collects radio measurements from the ground users every 0.1 second while the depth measurements are collected every 2 seconds. The Lidar sensor has the maximum range of $r_{\text{max}} = 150 \text{ m}$ and $\psi_{\text{max}} = 50$ degrees field of view. The mission time is assumed to be fixed and equals to 115 seconds.

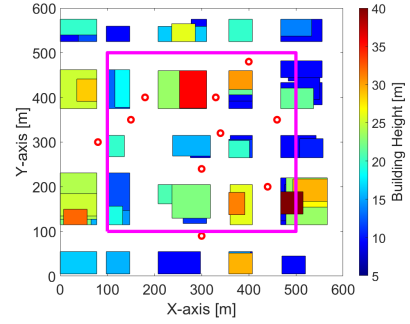


Fig. 4: Top view of the city and the UAV trajectory. Users are marked with circles.

In Fig. 5, we compare the map reconstruction performance of the proposed algorithm (fusing depth and radio measurements) to that of a case where only depth measurements are used, for the system setting shown in Fig. 4. The UAV follows a square trajectory and 10 users are randomly scattered over the city as depicted in Fig. 4. We also show the true and the estimated radio map for a given user which is located at $\mathbf{u} = [180, 400, 0]^T \text{ m}$. We can see that there is considerable improvement in the estimated maps with the fusion of depth and radio measurements. Note that, the radio map is reconstructed for a fixed altitude of 60 m.

To compare the performance of the algorithms in an average sense, an average root mean square error (ARMSE) is used as the metric and it is given by

$$\mathcal{E} = \frac{1}{K} \sum_{k=1}^K \sqrt{\mathbb{E} \left\{ (\hat{g}(\mathbf{v}, \mathbf{u}_k) - g(\mathbf{v}, \mathbf{u}_k))^2 \right\}}, \quad (26)$$

where $g(\mathbf{v}, \mathbf{u}_k)$ is the true channel gain, $\hat{g}(\mathbf{v}, \mathbf{u}_k)$ is the estimated gain, and the expectation is taken over a set of random UAV locations. In Fig. 6, we show the ARMSE of the radio map estimation versus increasing the number of ground users. We also compare the results of our algorithm with [7], and an extension of [9]. In [7], the radio map is estimated just from the collected radio measurements by using the EM algorithm (no 3D map is reconstructed), while in [9] a 3D model of the city is constructed from the radio measurements. We then use this 3D map to estimate the radio map akin to Section IV. For further comparisons, we have computed the ARMSE of the radio map reconstruction when only the depth measurements are utilized for the 3D map construction. In this approach, the 3D map of the city is first constructed using the depth information and then the collected radio measurements are classified as follows

$$s_{n,k} = \begin{cases} \text{LoS} & \text{if } p_{n,k}(\rho_{n,k} = \text{LoS}) > 0.5 \\ \text{NLoS} & \text{else} \end{cases}, \quad (27)$$

where $s_{n,k}$ is the label of each measurement and $p_{n,k}(\rho_{n,k} = \text{LoS})$ is computed from (11). Having classified the measurements, the radio channel parameters are learned in each segment using maximum likelihood estimator [9]. The radio map then is estimated similar to Section IV. The performance

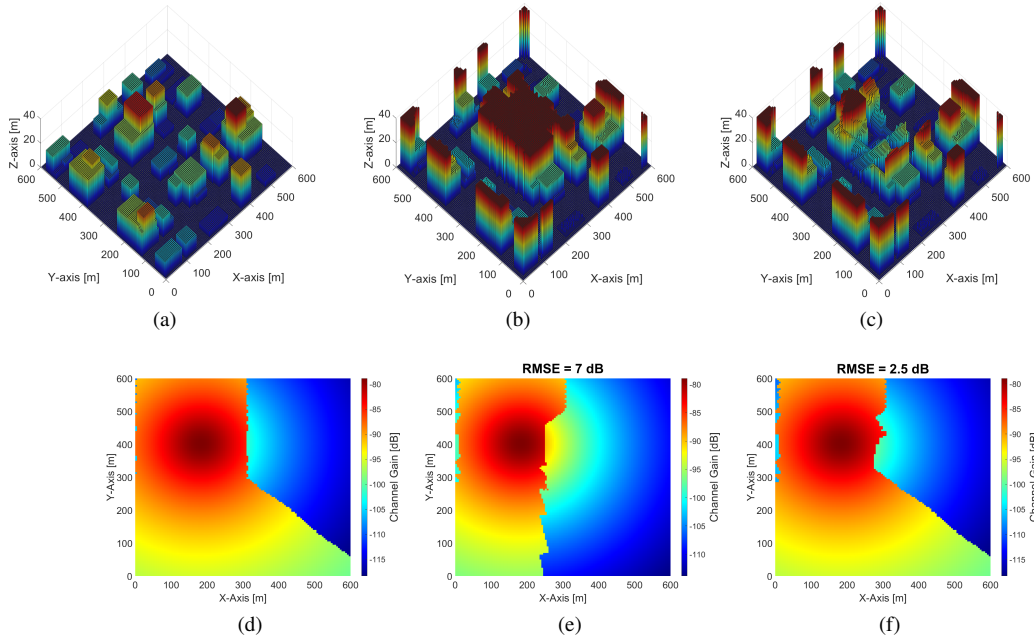


Fig. 5: For the system setting shown in Fig. 4, (a) True 3D city map. (b) Reconstructed 3D map using depth data. (c) Reconstructed 3D city map by fusing depth and radio measurements. (d) True radio map for a given user. (e) Estimated radio map from depth data for a given user. (f) Estimated radio map from depth and radio data for a given user.

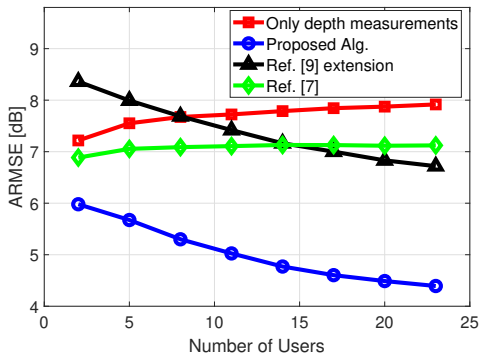


Fig. 6: Radio map estimation error vs. number of users.

of different approaches are compared over Monte-Carlo simulations with different user locations. Note that, in each run of the Monte-Carlo simulation, the users location are same for the measurement collection (3D map construction and channel learning) and for the evaluation (radio map estimation) phases. As it can be seen, our proposed algorithm outperforms other approaches. It is worth noting that, by increasing the number of users the estimation error decreases for both of our algorithm and the extension of [9]. Because in both approaches, the collected radio measurements are used to construct the 3D model of the city. Therefore, the more radio measurements we collect, the more precise 3D map estimation we can obtain which consequently improves the radio map estimation.

VI. CONCLUSION

We have investigated the problem of radio map estimation from the RSS and depth measurements obtained by a UAV

BS. The proposed approach consists of i) estimating the 3D map from the depth measurements, ii) fusing it with RSS measurements to refine the 3D map and learning the channel parameters, and iii) estimating the radio map. Numerical results show that fusion of radio and depth measurements significantly improves the map estimation.

REFERENCES

- [1] R. Gangula, O. Esrafilian, D. Gesbert, C. Roux, F. Kaltenberger, and R. Knopp, "Flying rebots: First results on an autonomous UAV-based LTE relay using Open Airinterface," in *IEEE SPAWC*, 2018.
- [2] A. Chowdhery and K. Jamieson, "Aerial channel prediction and user scheduling in mobile drone hotspots," *IEEE/ACM Transactions on Networking*, vol. 26, no. 6, pp. 2679–2692, 2018.
- [3] M. Mozaffari, W. Saad, M. Bennis, Y. Nam, and M. Debbah, "A tutorial on UAVs for wireless networks: Applications, challenges, and open problems," *IEEE Comm Surveys Tutorials*, vol. 21, no. 3, 2019.
- [4] Y. Zeng, Q. Wu, and R. Zhang, "Accessing from the sky: A tutorial on UAV communications for 5G and beyond," *Proceedings of the IEEE*, vol. 107, no. 12, pp. 2327–2375, 2019.
- [5] Q. Feng, J. McGeehan, E. K. Tameh, and A. R. Nix, "Path loss models for air-to-ground radio channels in urban environments," in *IEEE 63rd Vehicular Technology Conference*, May 2006.
- [6] A. Al-Hourani, S. Kandeepan, and A. Jamalipour, "Modeling air-to-ground path loss for low altitude platforms in urban environments," in *IEEE Global Communications Conference*, Dec 2014.
- [7] J. Chen, U. Yatnalli, and D. Gesbert, "Learning radio maps for UAV-aided wireless networks: A segmented regression approach," in *IEEE International Conference on Communications (ICC)*, 2017.
- [8] J. Chen, O. Esrafilian, D. Gesbert, and U. Mitra, "Efficient algorithms for air-to-ground channel reconstruction in UAV-aided communications," in *IEEE Globecom Workshops*, 2017.
- [9] O. Esrafilian and D. Gesbert, "3D city map reconstruction from UAV-based radio measurements," in *IEEE GLOBECOM*, 2017.
- [10] S. Thrun, W. Burgard, and D. Fox, *Probabilistic Robotics*. MIT Press, 2005.
- [11] 3GPP TR 38.901 version 14.0.0 Release 14, "Study on channel model for frequencies from 0.5 to 100 GHz," ETSI, Tech. Rep., 2017.